Cell Chemical Biology, Volume *27*

Supplemental Information

Regulation of MIF Enzymatic Activity by an Allosteric Site at the Central Solvent Channel

Georgios Pantouris, Leepakshi Khurana, Anthony Ma, Erin Skeens, Krystle Reiss, Victor S. Batista, George P. Lisi, and Elias J. Lolis

Supplementary Material

Regulation of MIF Enzymatic Activity by an Allosteric Site at the Central Solvent Channel

Georgios Pantouris[a*], Leepakshi Khurana[b], Anthony Ma[b], Erin Skeens[c], Krystle Reiss[d], Victor S. Batista[d], George P. Lisi[c*] and Elias J. Lolis[b,e*]

[a]*Department of Chemistry, University of the Pacific, Stockton, CA 95211, USA*

[b]*Department of Pharmacology, School of Medicine, Yale University, New Haven, CT 06510, USA*

[c]*Department of Molecular Biology, Cell Biology & Biochemistry, Brown University, Providence, RI 02903, USA*

[d]*Department of Chemistry, Yale University, New Haven, CT 06510, USA*

[e]*Yale Cancer Center, Yale School of Medicine, New Haven, CT 06510, USA*

[*]**Corresponding authors**

Georgios Pantouris, gpantouris@pacific.edu

George P. Lisi, george_lisi@brown.edu

Elias J. Lolis, elias.lolis@yale.edu

Supplementary Table 1. Data collection and refinement statistics for the Tyr99 and H62 mutants. Related to Table 1, Figures 2, 3.

	Y99F	Y99G	H62Y	H62F	H62A	H62G
Data collection						
Space group	P 21 21 21	P 21 21 21	P 21 21 21	P 21 21 21	P 21 21 21	P 21 21 21
Cell dimensions						
a, *b*, *c* (Å)	68.09, 68.11, 86.74	67.95, 68.08, 86.92	68.11, 68.31, 86.63	68.08, 68.26, 86.97	67.99, 68.22, 86.41	67.99, 68.21, 87.00
α, β, γ (°)	90.00, 90.00, 90.00	90.00, 90.00, 90.00	90.00, 90.00, 90.00	90.00, 90.00, 90.00	90.00, 90.00, 90.00	90.00, 90.00, 90.00
Resolution (Å)	50.00-1.53 (1.56-1.53) *	50.00-1.53 (1.56-1.53) *	50.00-1.73 (1.76-1.73) *	50.00-1.55 (1.58-1.55) *	50.00-1.61 (1.64-1.61) *	50.00-1.53 (1.56-1.53) *
R_{sym} or R_{merge}	0.035 (0.300)	0.048 (0.241)	0.041 (0.067)	0.047 (0.225)	0.054 (0.112)	0.052 (0.331)
I / σI	39.7 (4.1)	39.5 (5.5)	30.2 (10.2)	39 (6.4)	30.8 (7.7)	41.4 (4.7)
Completeness (%)	98.8 (95.0)	99.9 (99.2)	99.2 (99.5)	99.7 (98.7)	99.6 (96.9)	100 (99.8)
Redundancy	6.7 (4.3)	6.6 (4.2)	4.1 (2.2)	6.9 (4.5)	4.9 (2.5)	8.6 (5.4)
Refinement						
Resolution (Å)	48.16-1.53	48.09-1.53	48.23-1.73	48.21-1.55	48.16-1.61	48.15-1.53
No. reflections	57876	58529	40663	56183	49953	58470
R_{work} / R_{free}	0.15/0.17	0.15/0.18	0.15/0.18	0.12/0.15	0.15/0.18	0.11/0.16
No. atoms						
Protein	2649	2600	2585	2634	2585	2629
Ligand/ion	55	47	38	37	35	58
Water	345	316	321	327	384	349
B-factors						
Protein	13	13	18	15	12	14
Ligand/ion	25	24	31	74	22	29
Water	29	29	29	33	26	33
R.m.s. deviations						
Bond lengths (Å)	0.016	0.015	0.026	0.017	0.025	0.018
Bond angles (°)	1.760	1.832	2.047	1.751	2.141	1.759

Supplementary Table 2. The PDB entries, rmsd values to wild-type MIF, and resolution of the 19 structures with all three active sites occupied. Related to Figure 6.

PDB entry	RMSD (Å)	Resolution (Å)	Ligand Type	Ligands/MIF	Citation
3DJH	-	1.25	-	-	(Crichlow et al., 2009)
1CA7	0.20	2.5	Substrate (p-hydroxyphenyl pyruvate	3	(Lubetsky et al., 1999)
1GCZ	0.20	1.9	Competitive inhibitor	3	(Orita et al., 2001)
1LJT	0.22	2.0	Competitive inhibitor	3	(Lubetsky et al., 2002)
1MFI	0.36	1.8	Competitive inhibitor	3	(Taylor et al., 1999)
3L5U	0.27	1.9	Competitive inhibitor	3	(McLean et al., 2010)
4F2K	0.34	1.53	Covalent inhibitor	3	(Tyndall et al., 2012)
3B9S	0.36	1.8	Covalent inhibitor	3	(Winner et al., 2008)
3WNT	0.32	2.07	Covalent inhibitor	3	(Spencer et al., 2015)
3CE4	0.20	1.55	Covalent inhibitor	3	(Crichlow et al., 2009)
3SMB	0.28	1.6	Covalent inhibitor	3	(Crichlow et al., 2012)
3SMC	0.29	1.8	Covalent inhibitor	3	(Crichlow et al., 2012)
4OYQ	0.20	1.7	Covalent inhibitor	3	(Spencer et al., 2015)
3JSF	0.26	1.93	Covalent inhibitor	3	(McLean et al., 2009)
3JSG	0.25	1.58	Covalent inhibitor	3	(McLean et al., 2009)
3JTU	0.26	1.86	Covalent inhibitor	3	(McLean et al., 2009)
4P01	0.20	2.07	Covalent inhibitor	3	(Pantouris et al., 2015)
4TRF	0.29	1.63	Covalent inhibitor	3	(Pantouris et al., 2015)
4P0H	0.27	1.93	Covalent inhibitor	3	(Pantouris et al., 2015)
4PLU	0.22	1.63	Covalent inhibitor	3	(Pantouris et al., 2015)

Supplementary Table 3. Summary of critical hydrogen bonds involving Tyr99 during MD simulations. Related to Figures 4.

Acceptor	Donor	Mutation	Chain	Hydrogen Bonds/Frame	Average
Met2	His62	WT	A	0.73	0.71
			B	0.71	
			C	0.70	
		Y99A	A	0.60	0.66
			B	0.75	
			C	0.62	
		Y99G	A	0.67	0.71
			B	0.75	
			C	0.71	
		H62G	A	0.63	0.58
			B	0.54	
			C	0.58	
His62	Met2	WT	A	0.84	0.83
			B	0.85	
			C	0.81	
		Y99A	A	0.83	0.85
			B	0.86	
			C	0.86	
		Y99G	A	0.85	0.84
			B	0.85	
			C	0.82	
		H62G	A	0.72	0.68
			B	0.70	
			C	0.62	
Ser63	Tyr99	WT	A	0.38	0.38
			B	0.36	
			C	0.40	
		Y99A	A	0.31	0.32
			B	0.34	
			C	0.31	
		Y99G	A	0.31	0.29
			B	0.31	
			C	0.24	
		H62G	A	0.22	0.21
			B	0.23	
			C	0.17	
Tyr99	Leu61	WT	A	0.75	0.75
			B	0.77	
			C	0.74	
		Y99A	A	0.70	0.69
			B	0.67	
			C	0.70	
		Y99G	A	0.77	0.71
			B	0.69	
			C	0.66	
		H62G	A	0.72	0.68
			B	0.72	
			C	0.61	

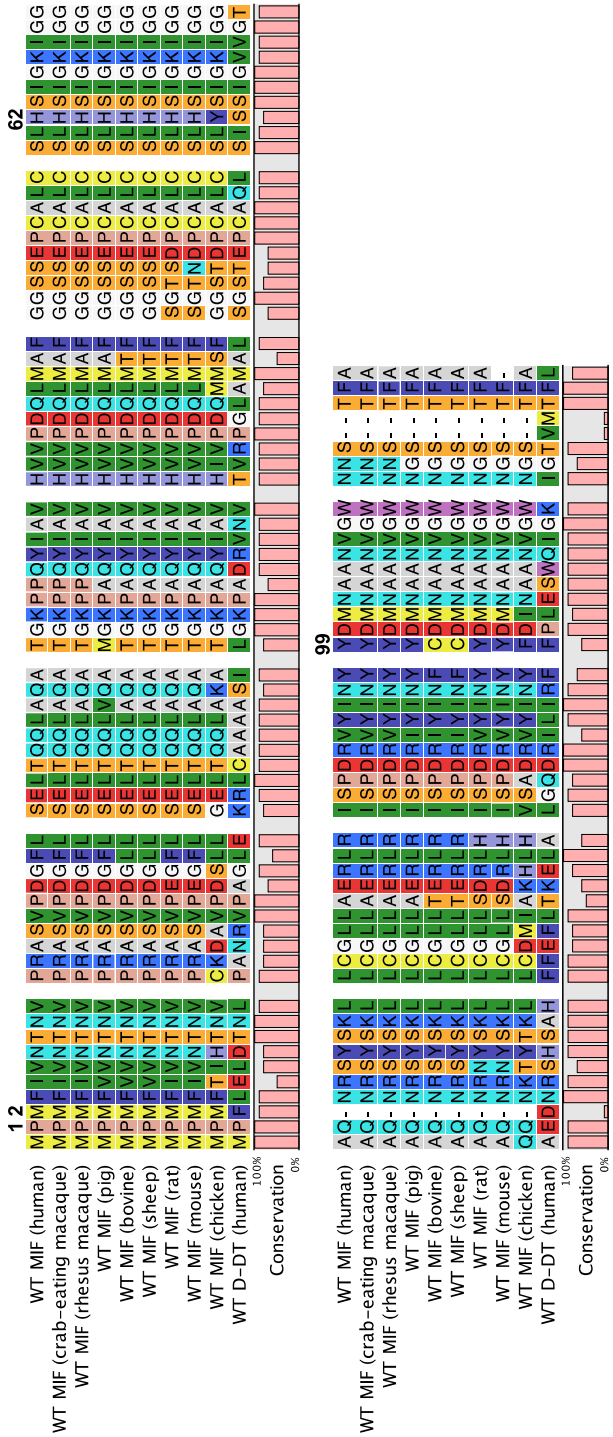

Supplementary Figure 1. Sequence alignment of human D-DT with homologues of WT MIF. Residues that comprise the solvent channel allosteric pathway (Pro1, Met2, His62, and Tyr99) are indicated above the sequences. These sites are highly conserved among MIF homologues. Despite structural and functional similarities between MIF and D-DT, including the conserved Pro1, D-DT does not share the allosteric residues characterized in this pathway, nor does it share the CD74 activation residues. Related to **Figure 1**.

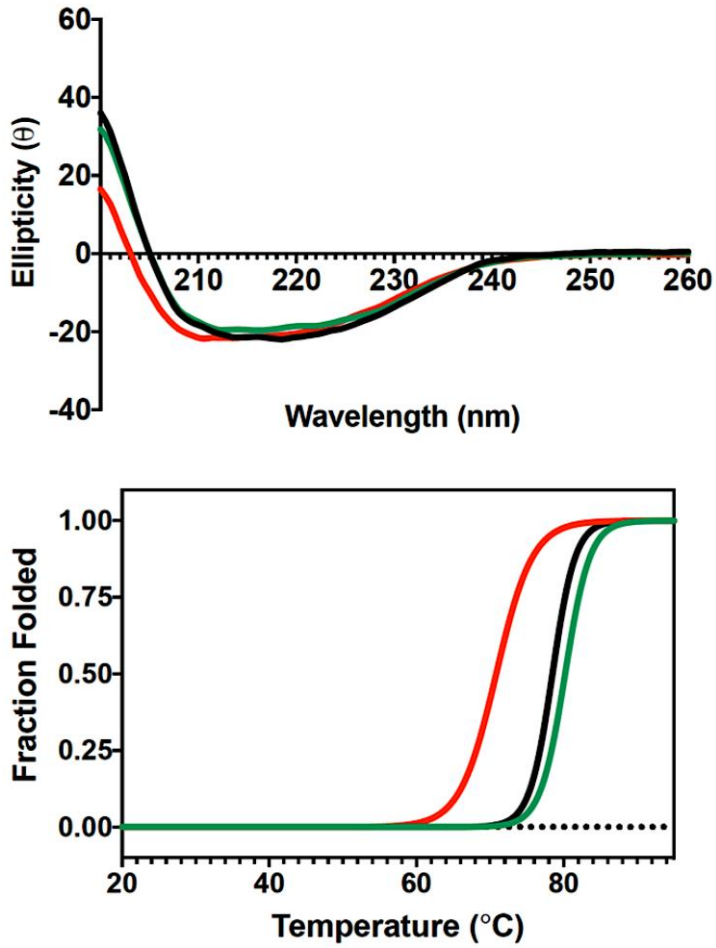

Supplementary Figure 2. Circular dichroism spectra (top) of WT (black), Y99G (red), and Y99F (green) MIF. Thermal unfolding experiments for these mutants (bottom) are plotted as a normalized fraction folded. Denaturation curves of 15 – 20 μM MIF were recorded at 218 nm in a 1 mm quartz cuvette. The temperature range for each scan was 20 – 90 °C (293 K – 363 K). Thermodynamic parameters shown in the table below were extracted via nonlinear curve fitting of CD data using GraphPad Prism as:

$$Ellipticity\ (T) = \frac{[(m_f T + b_f) + (m_u T + b_u)]exp\left[\left(-\frac{\Delta H_{D,vH}}{R}\right)\left(\frac{1}{T} - \frac{1}{T_m}\right)\right]}{1 + exp\left[\left(-\frac{\Delta H_{D,vH}}{R}\right)\left(\frac{1}{T} - \frac{1}{T_m}\right)\right]} \quad (1)$$

Where m_f, b_f, and m_u, b_u are the slopes and y-intercepts of the folded (low temperature) and unfolded (high temperature) regions of the melting curve; R is the gas constant; T_m and $\Delta H_{D,vH}$ are the unfolding midpoint and van't Hoff enthalpy of denaturation at T_m, respectively.

Free energy analysis was performed with calculated values of ΔC_p, the unfolding heat capacity, estimated from the report of Privalov and Makhatadze (Privalov and Makhatadze, 1990) with a contribution of ~ 14 cal/molK. The apparent differences in unfolding enthalpy, entropy, and free energy between these MIF variants was calculated as using a reference temperature (T_{REF}) of 351.9 K, the T_m of WT MIF.

$$\Delta H_{D,app} = \Delta H_{D,vH} + \Delta C_p (T_{REF} - T_m) \quad (2)$$

$$\Delta S_{D,app} = \frac{\Delta H_{D,vH}}{T_m} + \Delta C_p ln\left(\frac{T_{REF}}{T_m}\right) \quad (3)$$

$$\Delta G(T) = \Delta H_{D,vH}\left(1 - \frac{T_{REF}}{T_m}\right) + \Delta C_p\left[(T_{REF} - T_m) - T_{REF} ln\left(\frac{T_{REF}}{T_m}\right)\right] \quad (4)$$

Protein	ΔT_m	[a]$\Delta\Delta G_D$ (kcal/mol)	[a]$\Delta\Delta H_D$ (kcal/mol)	[a]$\Delta\Delta S_D$ (kcal/mol)
WT MIF	0	0	0	0
Y99G MIF	(-) 7.1	(-) 3.77	(-) 5.18	(-) 1.21
Y99F MIF	(+) 1.8	(+) 0.959	(+) 1.77	(+) 0.811

[a]per trimer, calculated using ΔC_p = 4.8 kcal/molK for the MIF trimer (114 residues per monomer, 342 residues total) and a reference temperature of 351.9 K, the T_m of WT MIF (thus, $\Delta\Delta G_D$ for WT MIF = 0). Related to **Figures 2-3**.

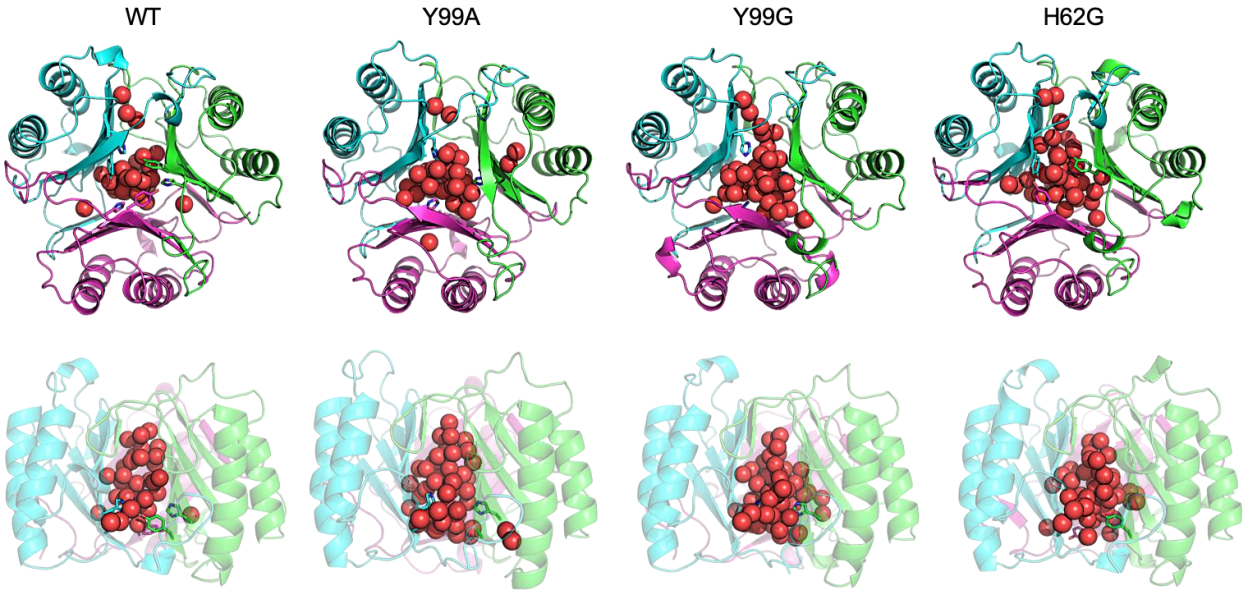

Supplementary Figure 3. Models from 200 ns MD simulations examining hydrogen bond networks in WT, Y99A, Y99G, and H62G MIF. Water molecules within the solvent channel, as well as hydrogen bond donor-acceptor distances between gating residues Y99 and V42 (top and bottom of channel) were used to determine the number of central water molecules in each MIF model. Related to **Figure 4**.

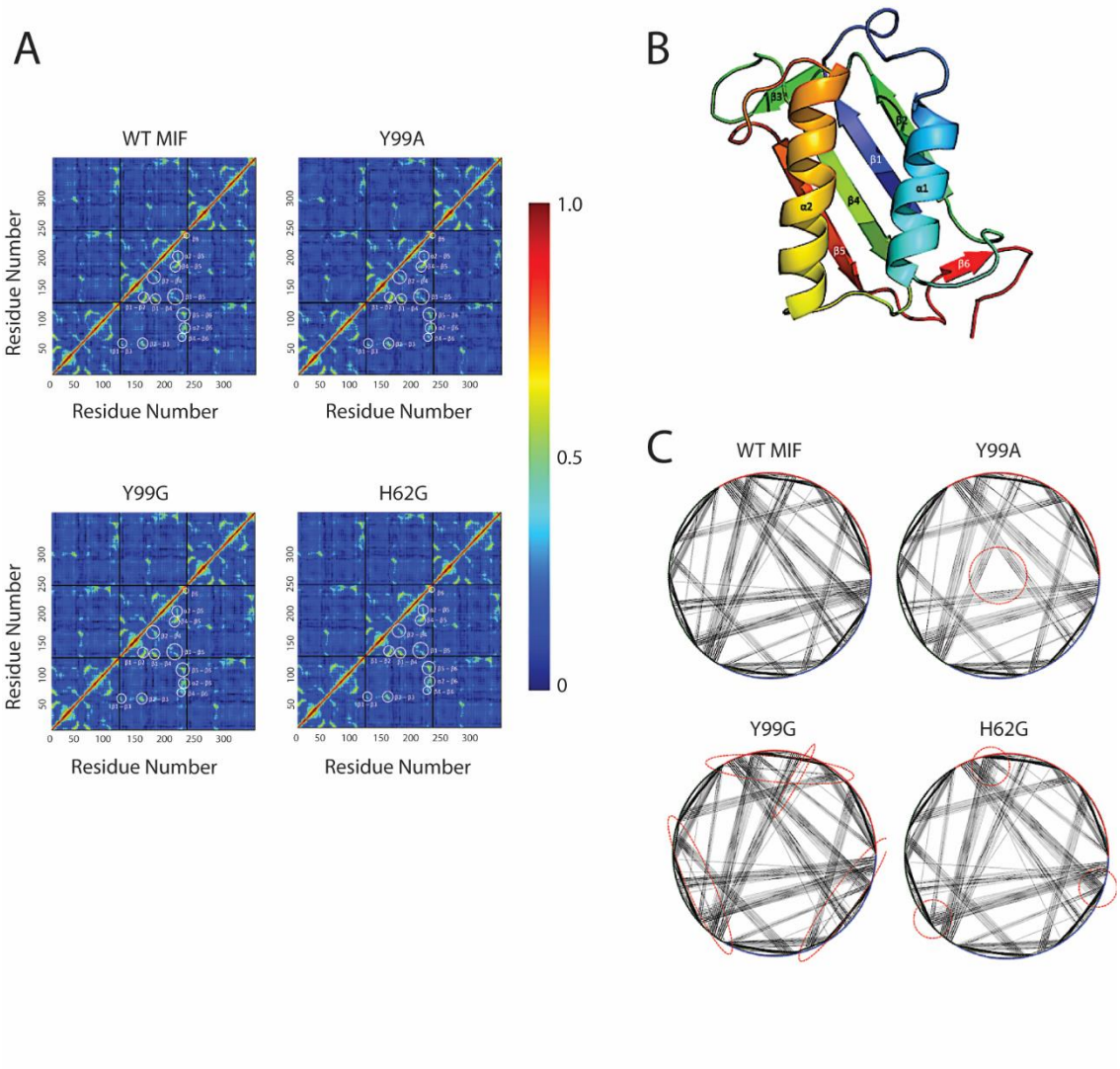

Supplementary Figure 4. Heat maps and community networks for WT MIF, Y99A, Y99G, and H62G mutations. (A) MIF intra-residue correlation during 200 ns MD simulations quantify RMSF values from alpha carbons of aligned trajectories. Each square within the map represents one of the MIF monomers (*i.e.* A, B, or C; bottom-to-top, and left-to-right). The diagonals show the A → A, B → B, and C → C correlations. Red indicates strong correlation between structural elements, while blue indicates little-to-no correlation. (B) Critical secondary structure elements are shown on the MIF monomer and circled in the correlation maps. (C) The MIF trimer is represented as a circle, with the red, blue, and green perimeters defining each of the MIF monomers. Black lines depict intra- and inter-monomer crosstalk, and red circles illustrate significant differences in mutants relative to WT. For example, correlations at the central solvent channel of Y99A (middle of circle) are weakened relative to WT, while inter-monomer correlations are fragmented in Y99G and H62G. Graphs were made using the NetworkX Python library (Hagberg et al., 2008). Related to **Figures 3-4**.

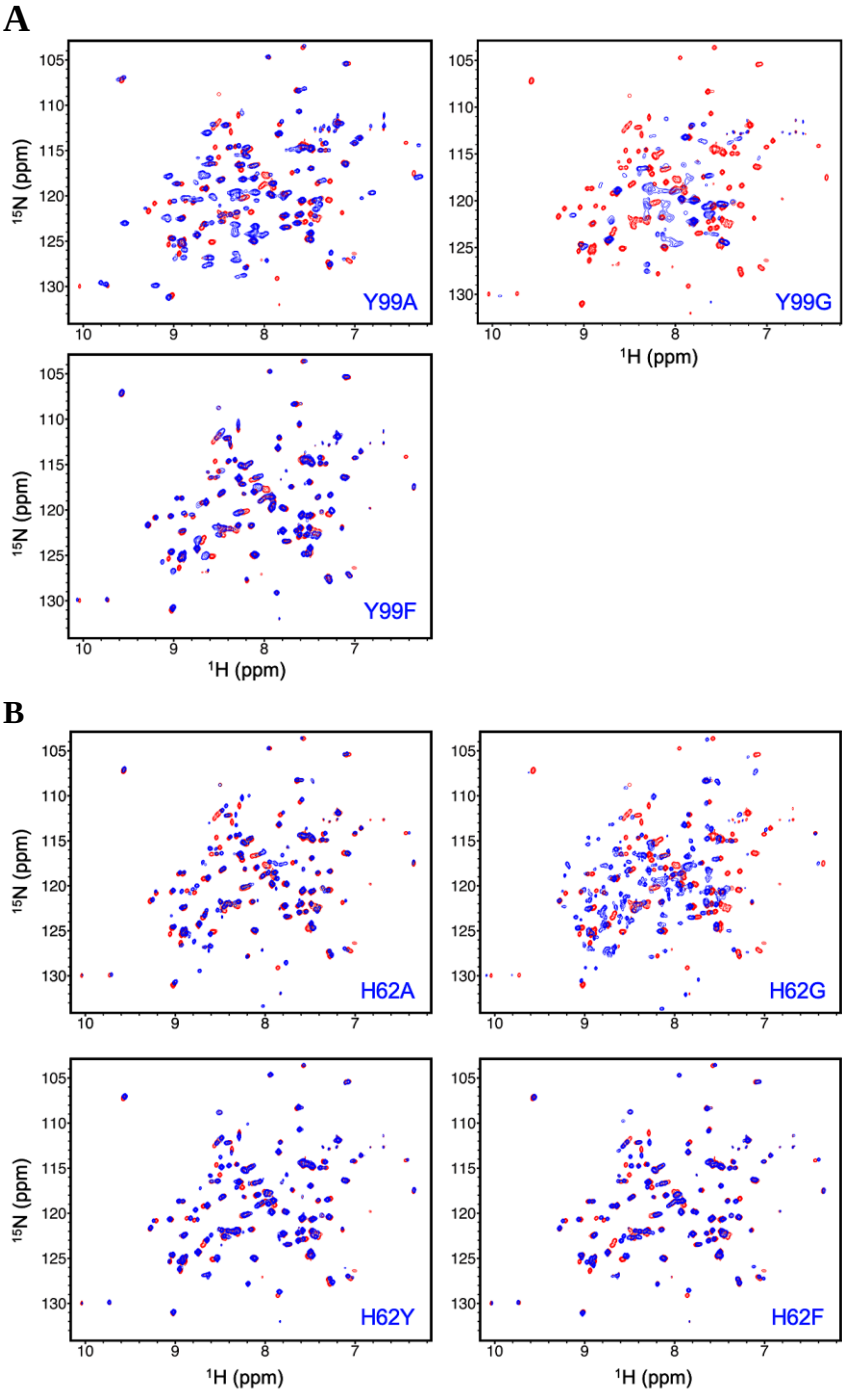

Supplementary Figure 5. ^{1}H-^{15}N TROSY HSQC NMR spectral overlays of Tyr99 (blue) and H62 mutants (blue) compared to WT MIF (red). (A) Overlays of Tyr99 (blue) mutants with WT MIF (red). (B) Overlays of His62 mutants (blue) with WT MIF (red). Chemical shift perturbations are summarized in the related **Figure 5A**.

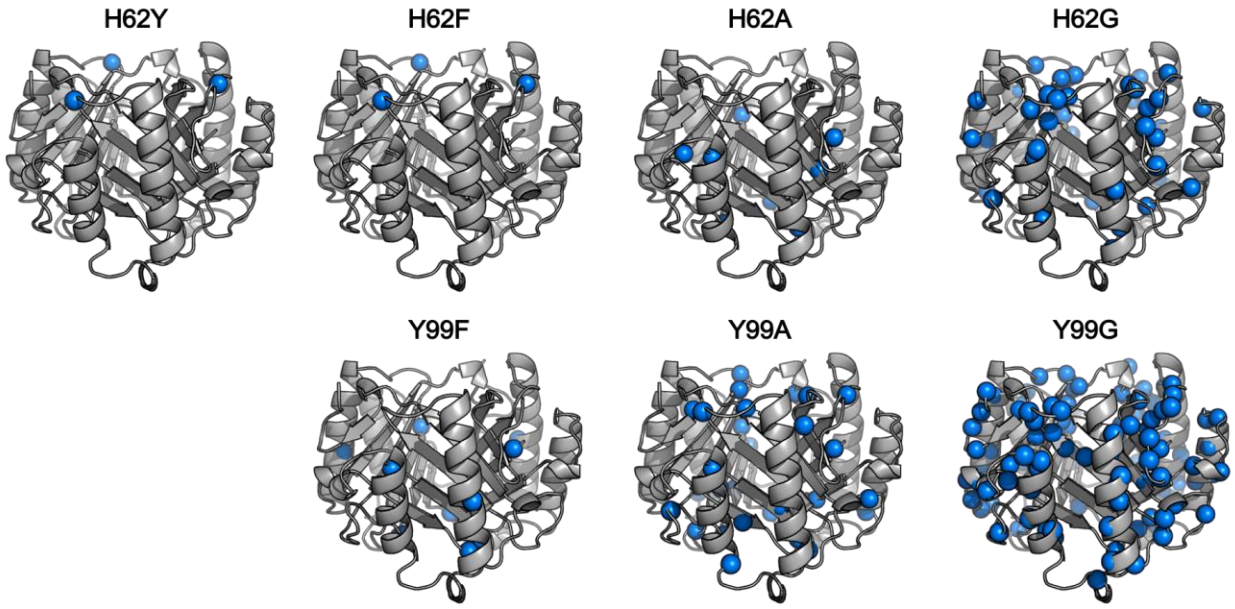

Supplementary Figure 6. Summary of amino acids broadened beyond detection (blue spheres) in ^{1}H-^{15}N NMR spectra of MIF mutants. The degree of line broadening increases from F/Y →A→ G mutations, and qualitatively denotes sites within MIF with heightened flexiblity on the *ms* timescale. Related to **Figure 5**.

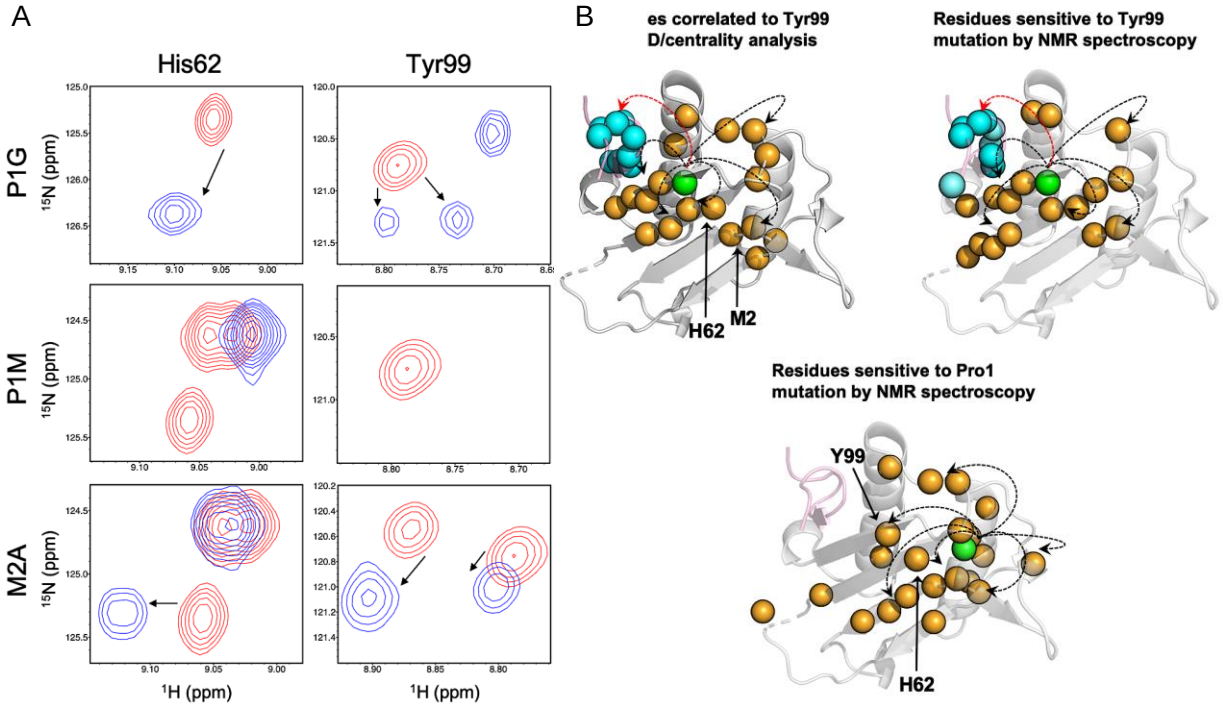

Supplementary Figure 7. (A) Allosteric reciprocity of the tautomerase and solvent channel sites. NMR studies of P1G, P1M, or M2A mutants shows significant chemical shift perturbations or line broadening at the Tyr99 allosteric site and His62 node. **(B)** Summary of correlated residues in MIF by MD and NMR. Residues identified to be correlated with Tyr99 in Pantouris, *et al*, (Pantouris et al., 2018) are mapped onto the MIF monomer (top left). Tyr99 is shown in green, and residues belonging to the C-terminus of the adjacent monomer are shown in cyan. Most of these correlations are also observed in NMR studies of Y99A MIF (top right, see also **Figure 5**), where spheres represent residues showing line broadening or chemical shifts 1.5σ above the 10% trimmed mean of all shifts. Residues sensitive to Pro1 mutations by NMR, however, show correlations at the Tyr99 allosteric site (bottom center, see also **Supplementary Figure 5A**), but **not** the C-terminal CD74 activation region. These data suggest Try99 is a critical node in both pathways, but may not enable direct concerted crosstalk between these sites. This is consistent with the different levels of attenuation of tautomerase (this work) and neutrophil recruitment (Pantouris et al., 2018) activity by the Y99A mutant. Related to **Figure 5**.

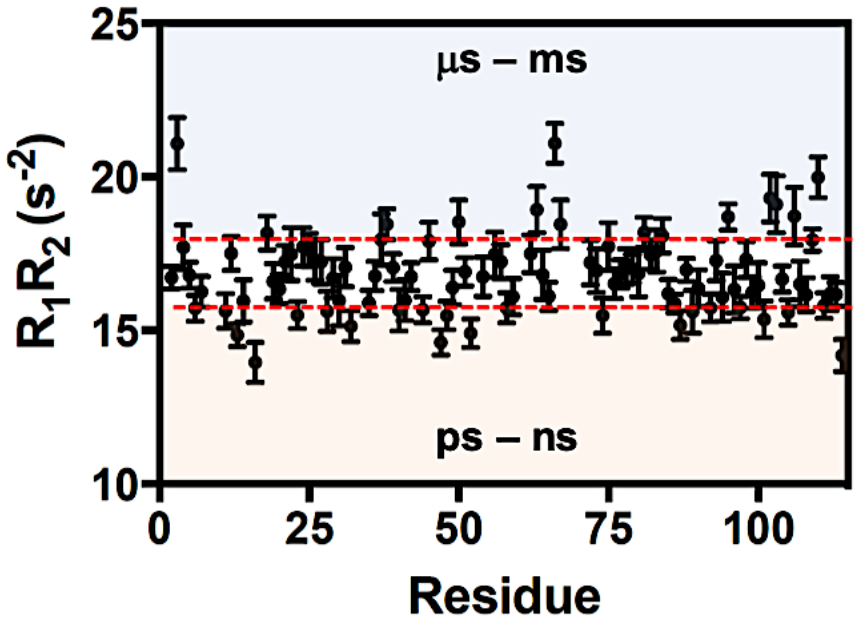

Supplementary Figure 8. NMR spin relaxation rates for wild-type MIF. The longitudinal (R_1) and transverse (R_2) relaxation rates are plotted as the R_1R_2 product, showing clear sites of micro-millisecond (1.5σ above the 10% trimmed mean, red dashed line) and pico-nanosecond chemical exchange (1.5σ below the 10% trimmed mean, indicating order parameter values significantly below the average S^2 = 0.85). These data indicate the wild-type MIF structure is intrinsically flexible on multiple timescales. Related to **Figures 5-7**.